Available online at www.sciencedirect.com
ScienceDirect
Catalysis Today 130 (2008) 345–353
CATALYSIS TODAY
www.elsevier.com/locate/cattod

Surface characterization of Al_2O_3–SiO_2 supported NiMo catalysts: An effect of support composition

Carolina Leyva, Mohan S. Rana, Jorge Ancheyta *

Instituto Mexicano del Petróleo, Eje Central Lázaro Cárdenas Norte 152, Col. San Bartolo Atepehuacan, D.F. 07730 Mexico

Abstract

Al_2O_3–SiO_2 mixed oxide has been investigated as a support for hydrotreating catalyst with variation of its composition [Si/(Si + Al) = 0.06, 0.12, 0.31, 0.56, 0.78] and its interaction with the surface active metals (NiMo). The composition of support and surface species (NiMo) of catalysts were characterized by specific surface area, atomic absorption, SEM-EDX, XRD, temperature programmed reduction (TPR), Raman analysis, scanning electron microscopy (STEM) and transmission electron microscopy (TEM). Incorporation of SiO_2 in Al_2O_3 promotes a weak interaction between the active phases and particularly catalyst that predominated with SiO_2 content. The oxide and sulfided catalysts characterization indicated that the effect of support is responsible to form different catalytic sites. Crystallization of MoO_3 phases and a relatively longer crystal of MoS_2 in the sulfided catalyst were attributed to an increasing SiO_2 content in the support. The catalytic behavior of the NiMo supported catalysts is explained in terms of structural changes on the surface due to the support and active metal interactions. The activity of the different catalysts evaluated in the thiophene hydrodesulfurization reaction was higher for the catalyst having lower SiO_2 content in the support.

Keywords: NiMo/SiO_2–Al_2O_3; Support effect; STEM; Raman; XRD; TPR; HRTEM; Metal sulfides

1. Introduction

In order to prepare effective hydrotreating catalysts to meet the challenge of environmental regulations to reduce sulfur, several approaches are in vogue, among which variation of support is an important one, which is responsible of the nature and dispersion of catalytic sites. Generally, SiO_2 supported hydrotreating catalysts are known to be less active for hydrotreating reactions compared with conventional Al_2O_3 supported catalysts, but they have better textural properties and possess some acidity on the support [1]. Therefore, it is felt that the combination of these two oxides as a support could have a synergistic impact on hydrotreating and such properties make them potentially attractive particularly as a support for hydroprocessing of heavy oil catalysts [2]. However, silica has been known for its poor dispersion of molybdenum phase [3]. That is the reason why alumina is used principally as a commercial support because it is economically favorable and has capability to acquire high dispersion of MoS_2.

Silica–alumina supported NiMo catalysts have been used for deep hydrodesulfurization of gas oil in which silica also favors the hydrodenitrogenation [4,5]. Generally, the amorphous SiO_2–Al_2O_3 support is used for hydrocracking catalysts due to its favorable acidity [6,7]. The major problem when using these acid materials for hydroprocessing applications is their high tendency to coke formation, which reduces catalyst activity with time-on-stream. The effect of silica support on hydrotreating catalyst has been reported using different composition, methods of preparation, evaluation with different feeds, etc. in the literature either alone or mixed with alumina [8–10]. The combination of two oxides (Al_2O_3 and SiO_2) has amorphous nature and a wide assortment of Brønsted and Lewis acid sites, which provide a greater acidity than that of individual alumina or silica. Moreover, the low isoelectric point (IEP, i.e., ≈2.5) of SiO_2 can be enhanced by adding alumina that improves interaction between support and active metals [11]. The interactions of active phases are further responsible of catalytic activity. Since alumina has higher IEP (i.e., ≈8), thus, it is

* Corresponding author at: Instituto Mexicano del Petróleo, Eje Central Lázaro Cárdenas 152, D.F. 07730 Mexico. Tel.: +52 55 9175 8443; fax: +52 55 9175 8429.
E-mail address: jancheyt@imp.mx (J. Ancheyta).

0920-5861/$ – see front matter © 2007 Elsevier B.V. All rights reserved.
doi:10.1016/j.cattod.2007.10.113

necessary to find out the detailed effect of surface species that are carried out by the SiO_2–Al_2O_3 mixed oxide support. The isoelectic point or zero point charge (ZPC) of Al_2O_3–SiO_2 (50/50, w/w) was reported in literature to be at around 6–7.5 [12–14]. The structural information of supported (Ni and Mo) phases can be obtained by XRD, Raman, temperature programmed reduction (TPR) on oxide state while the dispersion of supported MoS_2 phases can be confirmed by TEM [15].

The role of SiO_2 in improving the performance of catalysts is not clearly understood but it has been widely reported that increased acidity of silica–alumina support improves catalyst performance particularly for deep HDS of diesel fuel [16]. Moreover, it is also well known that hydrotreating catalyst undergoes large structural changes during the sulfidation [17] which depend on the nature of support as well as the preparation method of the catalysts [18]. Particularly in the case of SiO_2–Al_2O_3, Makishima et al. [19] reported that increasing the silica content in the support suppresses the growth of WS_2 slabs. Although the characterization and reactivity studies of supported SiO_2–Al_2O_3 catalysts have been the topic of several papers [20–22], detailed studies on the Mo and Ni species interaction with variation of support composition have been scarce, which depends on the support IEP variation as well as impregnation pH of the solution.

The aim of this study is to find out the nature of supported species in oxide as well as sulfide state and support effect on the dispersion of MoS_2, Ni–S phases and thiophene hydrodesulfurization. An increasing SiO_2 content in the support promotes the crystallization of MoO_3 phases, and a relatively longer crystal of MoS_2 in the sulfided catalysts. In order to estimate the interaction between support and active metals (Ni and Mo species), the catalysts were characterized in oxide as well as sulfide states.

2. Experimental

The support composition was varied by adjusting the amounts of aluminum nitrate and sodium silicate solution [Si/(Si + Al) = 0.06, 0.12, 0.31, 0.56, 0.78, w/w]. The SiO_2–Al_2O_3 supports were obtained by sol–gel homogeneous co-precipitation method using NH_4OH as precipitating agent. The aqueous solutions were mixed together slowly with controlled pH (2.5–9) and the precipitate was aged over night at 60 °C (pH ≈8.5) and filtered with the required amount of distilled water in order to wash Na^+ ions. The solid was dried at room temperature, 120 °C, and finally calcined at 550 °C for 4 h. These Al_2O_3–SiO_2 (AS) supports are labeled as AS-1(0.06), AS-2 (0.12), AS-3 (0.31), AS-4 (0.56), and AS-5 (0.78).

The nickel and molybdenum (NiMo) catalyst was prepared by the incipient wetness co-impregnation method in aqueous medium (pH ≈5.4) using appropriated amount of nickel nitrate and ammonium heptamolybdate. The impregnated catalysts were dried in air at 120 °C and calcined at 450 °C for 4 h. The supported catalysts are hereafter known as NiMoAS-1, NiMoAS-2, NiMoAS-3, NiMoAS-4, and NiMoAS-5.

The supports and catalysts were characterized by different techniques. BET specific surface area (SSA), total pore volume (TPV) and pore size distribution (PSD) were carried out in a Quantochrome Nova 4000 equipment using nitrogen gas at liquid nitrogen temperature (77 K). The composition of catalysts was studied by means of elemental analysis with an SEM-FIB analytical instrument xT Nova NanoLab 200, using SEM-EDX analysis. The sample was deposited on a carbon holder and evacuated at high vacuum (10^{-5} Torr) before images were taken. The nickel and molybdenum contents on catalysts were analyzed by atomic absorption spectrometry (ASTM D5863). Raman spectroscopy was applied for determining the nature of deposited species on catalysts using the laser power at the source of 514.5 nm and 5 mW. X-ray diffraction was performed on SIEMENS D-500 equipped with rotating and Cu Kα (λ = 0.15418 nm) radiation.

For TPR analyses an Altamira AMI-3 was used. A 20 mg sample of each promoted catalyst was reduced in a stream of H_2/Ar (10/90) at a flow rate of 30 ml/min, from 30 to 900 °C, analyzing the off gas by a TCD. Prior to each measurement the sample was preheated in a stream of Ar at 450 °C for 30 min to remove adsorbed water.

The sulfided catalysts transmission electron microscopy (TEM) was performed in JEM-2200FS transmission electron microscope with accelerating voltage of 200 kV. The microscope is equipped with a Schottky-type field emission gun and an ultra high-resolution configuration (Cs = 0.5 mm; Cc = 1.1 mm; point to point resolution, 0.19 nm) and in-column energy filter omega-type. Local chemical analysis and chemical mapping by energy dispersive X-ray spectrometry (EDX) was carried out in an energy dispersive X-ray spectroscope, NORAN, which is attached to the microscope and using the STEM-EDX combination. The samples were grounded, suspended in *n*-heptane at room temperature, and dispersed with ultrasonic agitation; then, an aliquot of the solution was dropped on a 3 mm diameter lacey carbon copper grid. Five different zones were estimated for STEM analysis and the selected size of zone was 50 nm. For TEM, at least 10 representative micrographs were taken for each catalyst in high-resolution mode. While an average length (L_{av}) and number of the stacks (N_{av}) of at least 120 slabs were measured for each catalyst.

The thiophene HDS reaction was conducted in a fixed-bed reactor operating at atmospheric pressure and interfaced with an online analysis at 400 °C with a flow of H_2/C_4H_4S mixture using a saturator temperature of 5 °C in order to have 4.7 mole% thiophene at the entrance of the reactor. Prior to HDS reaction, the catalyst was sulfided at 400 °C for 3 h in a flow of a CS_2/H_2 mixture. First-order rates were calculated according to the equation [$r = x(W/F)$], where r is the rate in mol h^{-1} $g_{cat.}^{-1}$, x the fractional conversion, W the weight of the catalyst in g, and F the flow rate of the reactant in mol h^{-1}. The particle sizes of the catalysts were 20–40 mesh and the conversions were kept below 15% to avoid diffusional limitations and operate under differential regime.

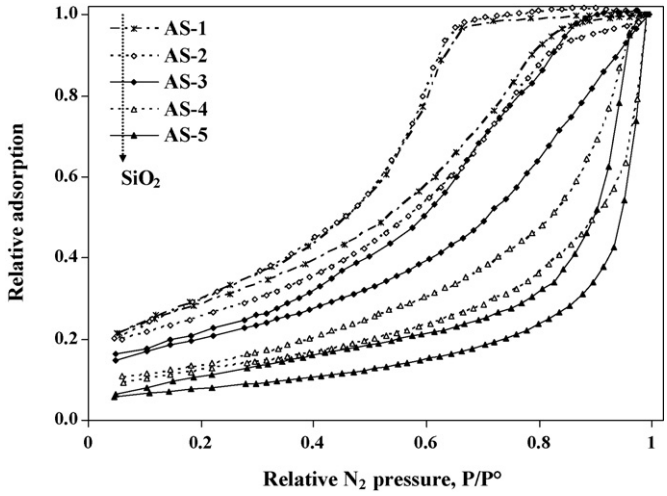

Fig. 1. Effect of support composition on the nature of textural properties of Al_2O_3–SiO_2.

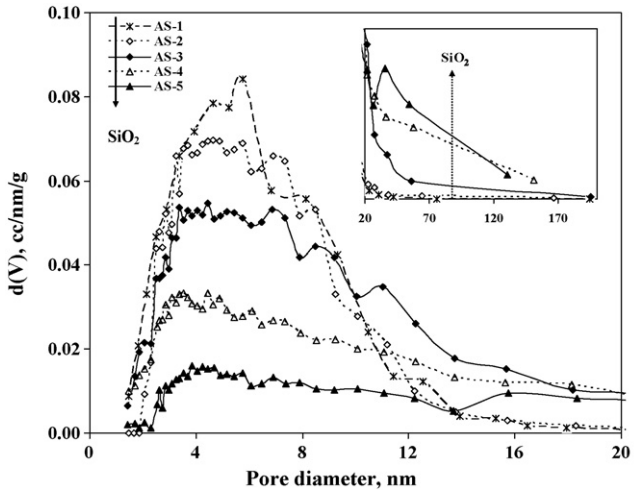

Fig. 2. Variation of pore diameter as a function of support composition of Al_2O_3–SiO_2.

Table 1
Textural properties of Al_2O_3–SiO_2 supports

Support	AS-1	AS-2	AS-3	AS-4	AS-5
SSA ($m^2\ g^{-1}$)	376	317	295	223	120
TPV ($cm^3\ g^{-1}$)	0.55	0.51	0.63	0.76	0.65
APD (nm)	6.2	6.6	8.4	13.7	21.8
Pore volume distribution (%)					
Micropore	0.8	0.2	1.4	1.3	0.3
Mesopore	98.5	97.8	94.2	71.1	66.5
Macropore	0.7	2.0	4.3	27.6	33.2
Pore size distribution (vol.%)					
<5 nm	35.3	33.2	20.9	12.3	5.7
5–10 nm	49.3	50.6	34.2	15.7	9.4
10–25 nm	13.5	12.2	31.5	23.9	20.1
25–50 nm	1.2	1.7	8.7	20.2	31.8
50–100 nm	0.5	1.3	2.3	4.3	21.8
>100 nm	0.2	1.1	2.3	23.5	11.1

SSA, specific surface area; TVP, total pore volume; APD, average pore diameter; AS, Al_2O_3–SiO_2.

3. Results and discussion

3.1. Characterization of support and catalysts

3.1.1. Textural properties and composition

The nitrogen adsorption–desorption isotherms of SiO_2–Al_2O_3 supports starting from low to high pressures are shown in Fig. 1. In the case of AS-4 and AS-5, the hysteresis loop is not very broad ($0.8 < P/P^\circ > 0.9$), which confirmed the macro-pore structure with large mono-modal pore distribution and low specific area of these solids, while the hysteresis loop of AS-1, AS-2 and AS-3 is relatively extended, which is typical of a solid of higher specific area and mesopores. The isotherms were of type IV (AS-1, AS-2, and AS-3) and II (AS-5) classification [23]. The specific surface area is calculated from adsorption data in the relative pressure range between 0.01 and 0.08. The textural properties of supports and catalysts are reported in Tables 1 and 2 respectively while pore size distribution of supports and catalysts are shown in Figs. 2 and 3 respectively. The total pore volume and pore size distribution were assessed from the amount of nitrogen adsorbed at a relative pressure (P/P°) of 0.9, assuming that the amount of the nitrogen condensed in the pores is equal to that of liquid nitrogen at 77 K. Wide range of differences were found for surface areas (376–120 $m^2\ g^{-1}$) and total pore volumes (0.5–0.7 ml/g), as the silica content was varied in the support. SSA decreased while the average pore diameter (APD) and TPV increased with increasing SiO_2 content. These tendencies of textural properties appear rater normal because macro-pore diameter of catalyst is increasing which enhances the TPV and decreases the SSA due to a decrease in micro- and meso-porous.

3.1.2. SEM-EDX, STEM and XRD analysis

The quantitative analyses of oxide catalysts were confirmed by SEM-EDX as shown in Fig. 4 and Table 3. The distribution

Table 2
Textural properties of catalysts

Catalyst	SSA ($m^2\ g^{-1}$)	APD (nm)	TPV (ml/g)	%Distribution of pore diameter		
				Micropore $d < 2$ (nm)	Mesopore $2 \geq d \leq 50$ (nm)	Macropore $d > 50$ (nm)
NiMoAS-1	327	5.8	0.48	1.1	98.3	0.6
NiMoAS-2	349	5.6	0.49	1.7	97.6	0.7
NiMoAS-3	255	8.5	0.54	1.2	93.5	5.3
NiMoAS-4	167	14.0	0.58	1.4	73.9	24.7
NiMoAS-5	103	19.1	0.47	1.4	64.7	33.9

SSA, specific surface area; APD, average pore diameter; TVP, total pore volume; d, pore diameter.

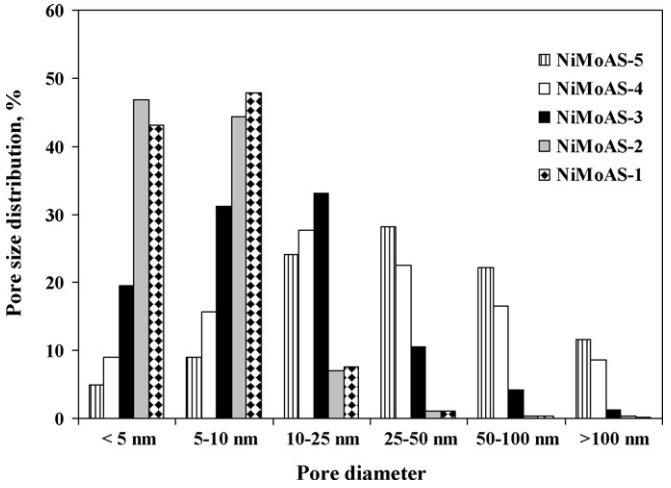

Fig. 3. Variation of pore diameter for Al_2O_3–SiO_2 supported catalysts with different silica content.

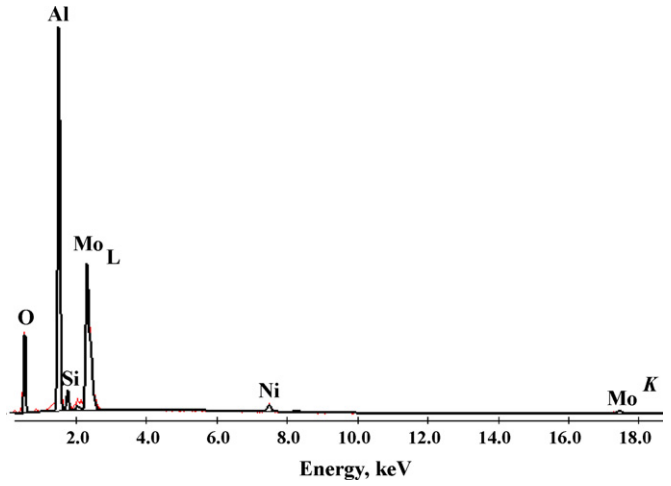

Fig. 4. EDX spectra of the oxide NiMo catalysts supported over Al_2O_3–SiO_2.

of SiO_2 and Al_2O_3 is homogeneous at the nanoscale, which was confirmed by scanning transmission electron microscopy (STEM) as shown in Fig. 5a and b. The qualitative element analysis of Si and Al estimated by STEM results indicated that the two components of support were distributed evenly, which decreases the possibility to aggregate the surface crystal of one component. The analyses were carried out for AS-3 and AS-4 supports and the density of elements (AlK and SiK) in mapping qualitatively represents the population of the elements compared with the whole image. The composition of catalysts was individually estimated as shown in Table 3. All catalysts contain similar amount of Ni and Mo, thus, theoretically all catalysts have the same number of catalytic sites. Even though the catalyst have the same amount of metals (Table 3), the nature of these oxidic species varies with the composition and/or nature of the support. Since the disparity is not sufficiently clear to allow a statistical count of the particle sizes; they are approximately in the same range. Thus, STEM analysis did not detect any obvious difference in particle size of silica (Si) and alumina (Al), which is in agreement with XRD results that are shown in Fig. 6. The X-ray diffraction pattern of supported catalysts are practically amorphous in nature, but at low silica content indications (at 2Θ, 46.1° and 66.8°) of alumina are shown while at higher content of silica the broad hump (at ≈2Θ 20°–23°) of amorphous silica is clearly noticeable. On the other hand the supported phases of MoO_3, NiO and its interacted phases (i.e., $NiMoO_4$) can be poorly seen particularly in the case of NiMoAS-5 catalyst. The poor intensities indicated that surface oxidic species (MoO_3 and NiO) crystal size exists either in less than 4 nm or they are well dispersed on high surface area supports. Moreover, the presence of crystalline $NiMoO_4$ is not evident by XRD.

Table 3
Catalyst composition determined by TEM-EDX

Sample	Support (wt.%)				Catalysts (wt.%)	
	Na_2O	Al_2O_3	SiO_2	Al/Si	Ni	Mo
NiMoAS-1	–	93.1	6.9	11.0	1.6	4.2
NiMoAS-2	–	85.4	14.6	6.4	1.8	5.2
NiMoAS-3	–	68.6	31.4	2.4	1.7	5.0
NiMoAS-4	0.8	43.6	55.6	0.8	1.7	4.2
NiMoAS-5	1.4	21.9	76.7	0.3	1.7	4.1

3.1.3. Raman spectroscopy

Raman analysis of NiMo supported catalyst has been an important technique to discriminate the different surface species of oxidic catalysts, whose spectra are shown in Fig. 7. The principal intensities are observed at 81.9, 816 and 993 cm^{-1}, those bands are assigned to the MoO_3 vibrations [24,25]. However, other intensities like 115, 158, 294, 339, 382, 667 cm^{-1} are relatively less affirmed and they also correspond to the MoO_3 phases. The diffusion of Ni species into the support (i.e. $NiAlO_4$) and NiO and its interaction with molybdenum ($NiMoO_4$) are not observed by Raman analysis that may be due to the very low loading of metal (≈4.5 wt.% Mo) as well as low calcinations temperature. A comparison of these spectra is made with pure NiO and $NiMoO_4$ as shown in Fig. 7 (inset). The Ni interactions in the support highly depend on the nature of support [25]. The absence of $NiMoO_4$ depends on the precipitation of surface metal species due to the large difference between the impregnation pH and IEP of support, since the IEP of Al_2O_3–SiO_2 is ca. 6.2 and the impregnation pH was around 5.4. Thus, it is more likely that after calcination, Mo–O–Mo species and MoO_3 crystallites are formed on the support surface. These results are in agreement with the presence of larger cluster particularly for NiMoAS-5 and NiMoAS-4 at around 82 cm^{-1}. Moreover, due to the low IEP of SiO_2 monomeric species can be easily polymerized ($Mo_7O_{24}^{6-}$ or $Mo_8O_{26}^{4-}$) at the SiO_2 surface, even at low molybdenum coverage [26]. Also, there is appearance of a relatively small band ca. 952 cm^{-1} in the high silica supported catalyst (NiMoAS-5), which may be attributed to the Mo=O bond of octahedral coordinated MoO_6 species [26]. Hence, it is expected that for pH (Mo impregnation solution) higher than IEP, anion adsorption easily occurs on the positively charge surface, while, if IEP is lower impregnation negatively charge

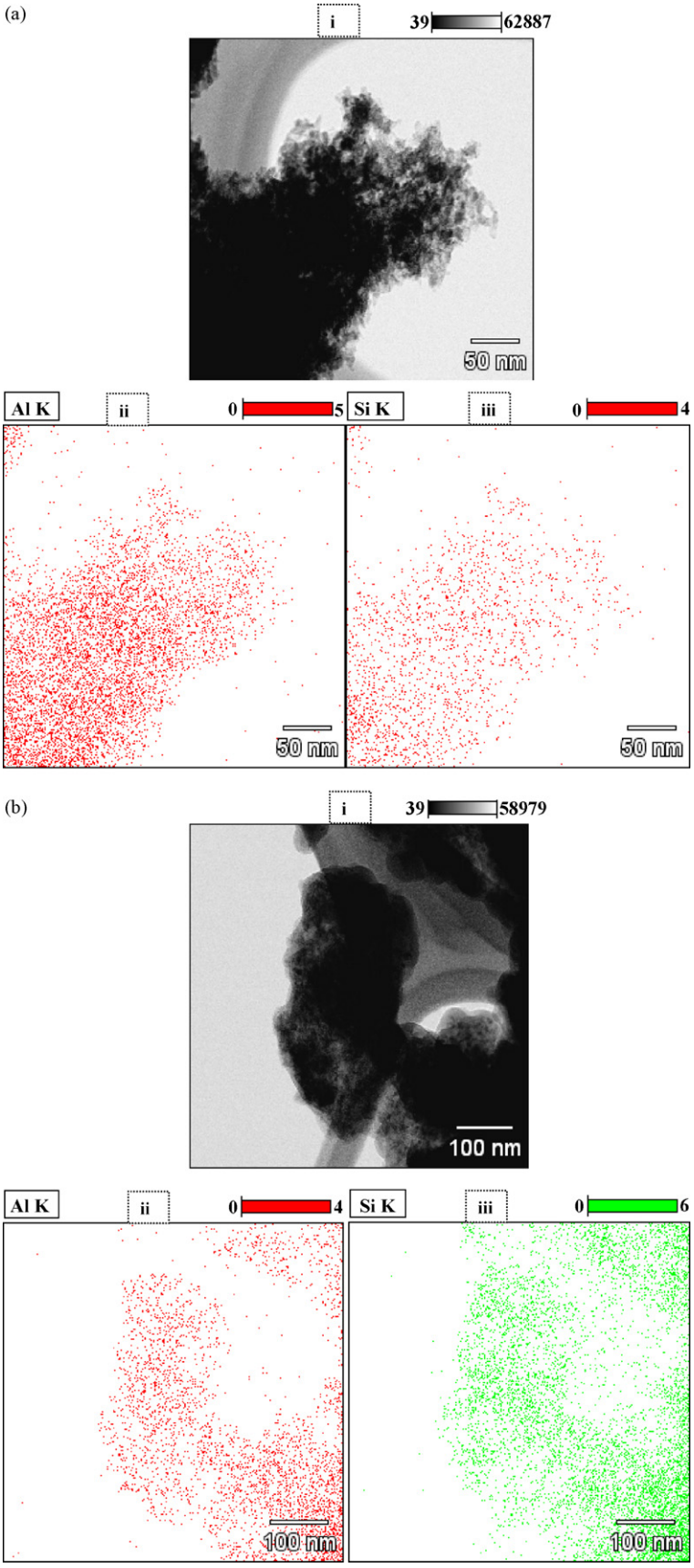

Fig. 5. (a) Scanning transmission electron micrographs (STEM) and qualitative nano-microanalysis of mixed oxide support (AS-3): (i) sample image, (ii) Al distribution, and (iii) Si distribution. (b) Scanning transmission electron micrographs (STEM) and qualitative nano-microanalysis of mixed oxide support (AS-4): (i) sample image, (ii) Al distribution, and (iii) Si distribution.

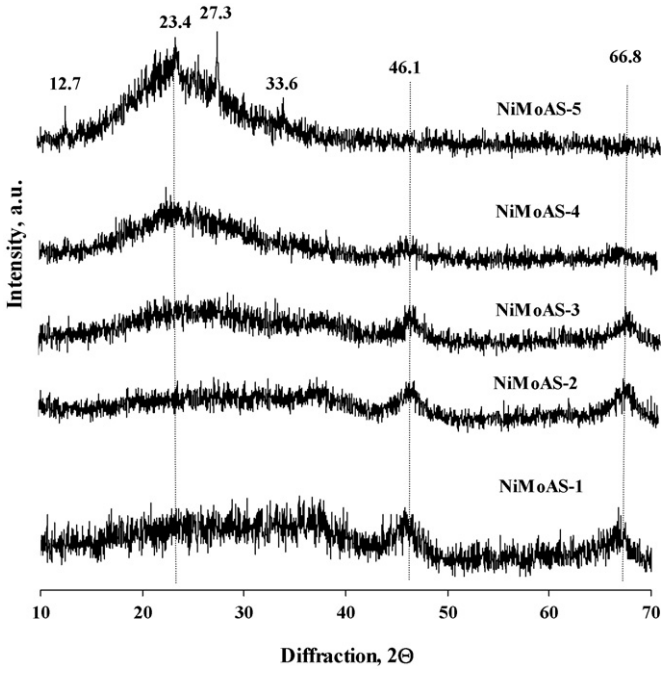

Fig. 6. XRD of NiMo/Al_2O_3–SiO_2 catalysts.

surface repulsion force existed between the support surface and molybdenum anions. Thus, the state of the surface molybdate species mechanism occurred in the wet state that depends on both the pH value of the impregnating solution (i.e., ≈5.4) and the point of zero charge (PZC) of the SiO_2–Al_2O_3 support. Hence, the coordination structure of the surface molybdate species and compensatory cations is a crucial factor for controlling the surface species.

3.1.4. Temperature programmed reduction (TPR)

To corroborate the above said interaction of surface species with the support, the corresponding TPR results are illustrated in Fig. 8a. The TPR results indicated that the surface species on Al_2O_3–SiO_2 widely modified the reduction behavior of molybdenum and nickel oxides with variation of support composition. Usually, the reduction of supported species (MoO_3) occurs in different steps ($MoO_3 \rightarrow MoO_2 \rightarrow Mo$). The

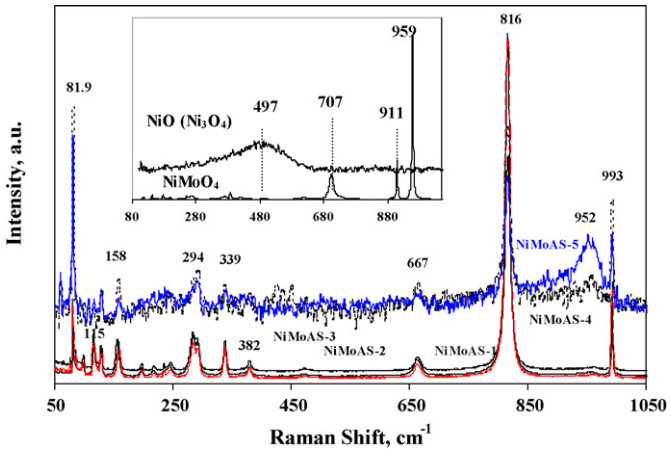

Fig. 7. Raman spectra of NiMo catalysts supported on Al_2O_3–SiO_2.

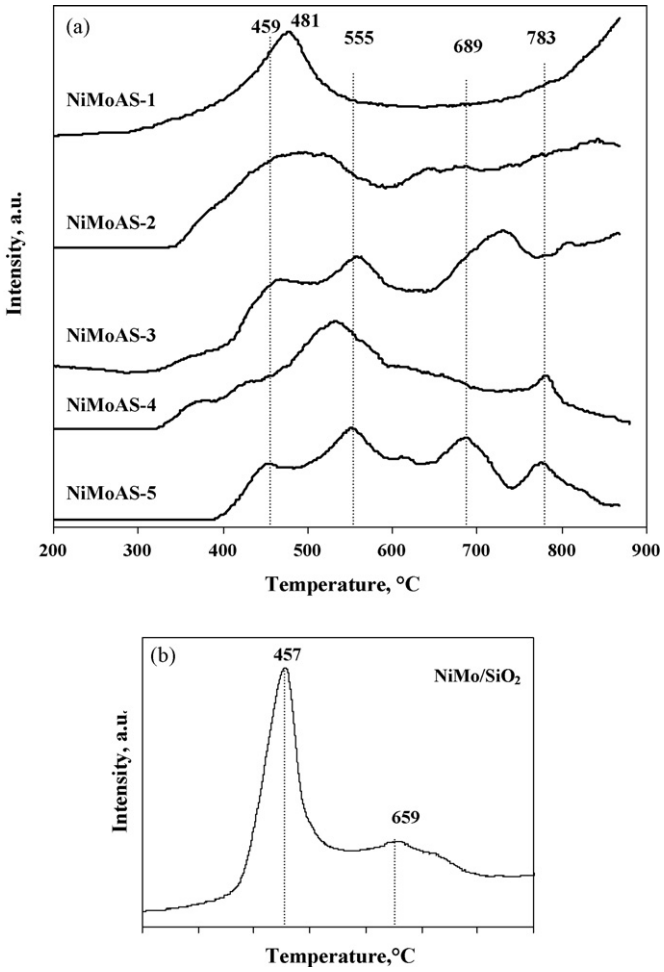

Fig. 8. TPR spectra of NiMo catalysts supported on (a) Al_2O_3–SiO_2, and (b) SiO_2.

low temperature peak at 481 °C is attributed to the partial reduction of Mo^{6+} to Mo^{4+} while subsequent peaks are the stepwise reduction of the bulk MoO_3. The low silica content catalyst only shows a reduction peak at 481 °C that can be attributed to molybdenum monolayer species, this peak is diminished as the content of silica increases, where Mo–Mo interaction is higher or the crystal size of surface species is greater, and these species are reduced at relatively higher and in various steps of temperature [27]. The stepwise reduction becomes more obvious as the silica content in support is increased where lower metal support interaction and larger crystal size of MoO_3 of multilayers of Mo oxide are expected. Since metal loading of these catalysts is very low so most of the Mo is distributed as a monolayer, but due to the silica very small amount of MoO_3 crystal aggregation may occur. The aggregated MoO_3 may also promote the Ni intermediate reducible species of Ni and Mo which may also be shown in the stepwise reduction peaks. The NiMo active phase over silica is reduced at lower temperature (Fig. 8b) and also the interaction between different support with NiMo (CoMo) has been reported recently [28]. Similar results are observed for amorphous SiO_2–Al_2O_3 supported NiMo catalysts explaining a nature of interaction between support and surface species

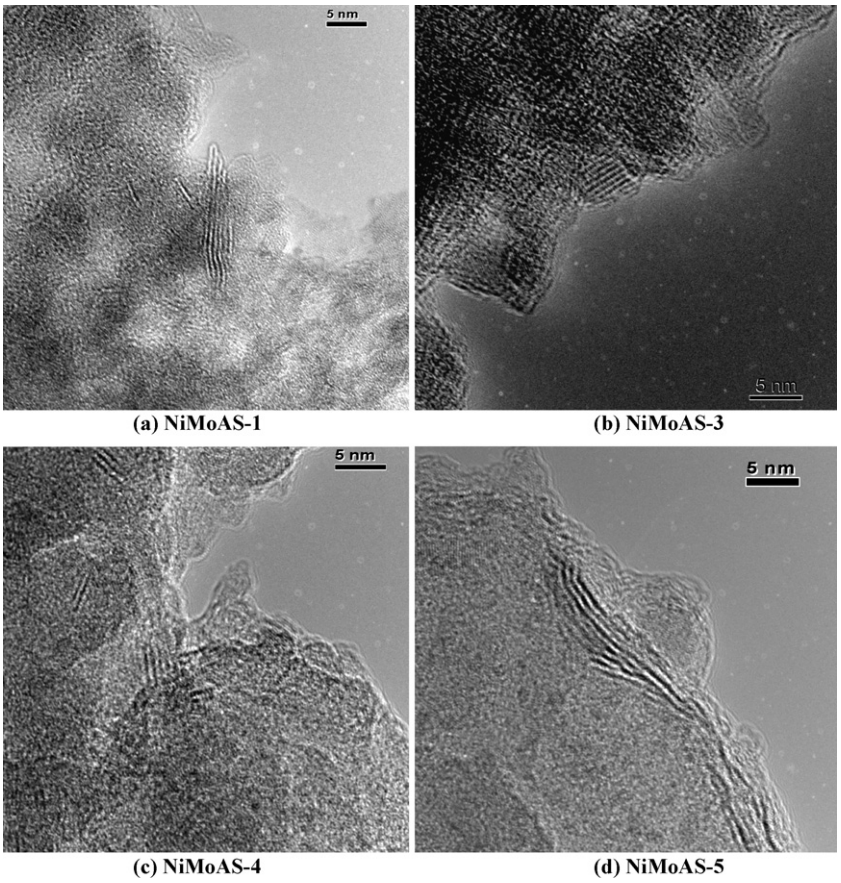

Fig. 9. HRTEM micrographs of NiMo supported catalysts over Al_2O_3–SiO_2: (a) NiMoAS-1; (b) NiMoAS-3; (c) NiMoAS-4; (d) NiMoAS-5.

characterized by NMR, TPR and HRTEM [15]. However, the interactions of support depend on different parameters such as isoelectric point of the support, impregnation pH as well as the number and strength of hydroxyl groups present on the surface of support [29].

3.1.5. High-resolution transmission electron microscopy (HRTEM)

Fig. 9 shows the HRTEM photographs of sulfided catalysts which represent the MoS_2 slab shape and size at different composition of support. The presence of various degrees of slab formation and length of its stacked layers on the support surface are likely affected by the sulfidation and consequently dispersion of Mo and Ni species. The low SiO_2 containing catalysts (NiMoAS-1, NiMoAS-2) demonstrated that an average length of MoS_2 is about 2.5 nm, while NiMoAS-3 has enhanced stacking of slabs but the average length remains around 3.1 nm. However, with further increase in the SiO_2 content the number of slabs as well as average length of MoS_2 increases. The average length (L_{av}) and number of layers (N_{av}) for the MoS_2 crystallites on different supports were estimated and are reported in Table 4. For low silica content in the support, the average length of MoS_2 crystallites is 2.5 nm, while an increase of silica in the support results in longer and more stacked MoS_2 crystallites. Similar results were reported for WS_2 stacking over the variation of SiO_2 composition in support [19]; however, the lateral growth was limited for the WS_2. An enhancement in stacking of MoS_2 further confirms the weaker interaction between support and molybdenum. High number of slabs and constant length indicate the presence of greater number of catalytic sites [15]. On the other hand if the lengths of MoS_2 increase that corresponds to the aggregated MoS_2 crystal, which has lower number of catalytic sites, and is indeed due to the weaker interaction with high silica containing support (as evident by formation of MoO_3) and that is responsible for high stacking of the MoS_2 slabs (evident by HRTEM).

3.2. Catalytic activity for thiophene HDS

The HDS activities of the NiMo supported catalysts are obtained from the conversion of thiophene with variation of SiO_2 content in the catalyst; the steady state HDS rate (after 4 h of reaction time) are reported in Table 5. A decreasing tendency

Table 4
Average length (L_{av}) and stacking (N_{av}) of MoS_2 crystallite over Al_2O_3–SiO_2

Catalyst	L_{av} (nm)	N_{av}
NiMoAS-1	2.5	1.2
NiMoAS-2	2.4	1.8
NiMoAS-3	3.1	2.2
NiMoAS-4	4.7	3.2
NiMoAS-5[a]	9.9	4.7

[a] Due to the nature of curve length the error may increase.

Table 5
Thiophene HDS reaction rate for SiO_2–Al_2O_3 supported NiMo catalysts with variation of support composition

Catalysts	Support composition, [Si/(Si + Al)]	r_{HDS}, (mol h^{-1} g^{-1}cat.)10^3
NiMoAS-1	0.06	10.3
NiMoAS-2	0.15	9.1
NiMoAS-3	0.31	8.5
NiMoAS-4	0.56	4.8
NiMoAS-5	0.78	3.5

of HDS activity was observed with increasing the SiO_2 content in the support. The catalyst containing lower silica content and smaller pore diameter is having much better HDS activity. Since all catalysts are having mesopores so the effect of pore diameter is not likely affecting the catalyst activity with such a great magnitude. Apart from the textural properties modification of support may vary the acidity of the catalyst, which may have some effect on HDS activity; the acidity of NiMo supported catalyst was found to be maximum for NiMoAS-4 [30], which also does not chase the HDS activity. Thus, the reason for dwindle in HDS activity is the support composition wherein SiO_2 plays an important role to direct catalytic sites, which leads to a decrease in catalytic activity by decreasing the Ni and Mo active sites. Significant activity variation suggests that the active sites existence due to anchoring of Mo atoms on Al_2O_3–SiO_2 compositions differs due to silica. The pure silica is characterized by a low point of zero charge that usually refers to specific adsorption of OH^- and H^+ ions [31]. The pure silica is having isoelectric point ≈2.5, while for pure alumina it is about 8, therefore, the co-impregnation pH of Mo and Ni kept around 5.4, i.e., in between IEP of both systems and in this way the support surface will be neutrally charged. At this Mo concentrations and pH values the polyanion of Mo is adsorbed on the surface, it is believed that this species has predominated by well dispersed molybdenum while increasing the SiO_2 in the support, the PZC of support decreases but the pH of impregnation solution (Ni and Mo) remains the same (i.e., 5.4) which leads to bulk MoO_3 formation after calcination.

The MoO_3 crystal formations are confirmed by the XRD and Raman and sulfided state by the HRTEM. In sulfided catalyst, the MoS_2 slab spacing (S–Mo–S) is about 0.616 nm and the unit is periodically repeated along the directions parallel to the support surfaces. The long slab length is further indicative to the low dispersion of MoS_2. Apart from this Ni atoms may be present in three forms after sulfidation such as Ni_3S_2 crystallites, nickel atoms on the edges of MoS_2 crystallites (i.e., Ni–Mo–S active phase) and as nickel cations at the support lattice (i.e., Al_{oct} or Al_{tet}). The lower activity of NiMoAS-5 catalyst may be due to the low dispersion of molybdenum but the crystals growth was poorly identified by the XRD and Raman analysis. However, the decrease in activity is almost three times lower. Thus, the Mo dispersion is not only the reason behind the activity decrease. The high-resolution TEM magnification shows an abnormal grain growth of disordered nanoparticles (NiMoAS-5) across the MoS_2 slabs, which are shown in Fig. 10. Moreover, the curved MoS_2 slab morphologies have been confirmed to the lower dispersion of MoS_2 [32–35]. Thus, the NiMoAS-5 curvature stacking is corresponding to the low dispersion of MoS_2 so the activity, which is usually a case of high silica catalyst. Apart from long and curved MoS_2 stacking an across stacking is typically observed for NiMoAS-5, which has maximum silica content in the support (76.7 wt.%). The distances between the cross slabs are of approximately 0.302 nm, which may contribute either Mo–Mo or Ni_xS_y type of phases. The sulfided catalysts different slab distances are reported for Ni–S (Ni presence in the edge sites) of 0.221 nm, Ni–Ni of 0.315 nm, Ni–Mo of 0.286 nm and Mo–Mo of 0.316 nm [36–38]. However, the distances also depend on the coordination number as well as flushing conditions [38]. These results indicated Ni either intercalated Ni–Ni or Ni–Mo, which leads to decrease a vast number of Ni

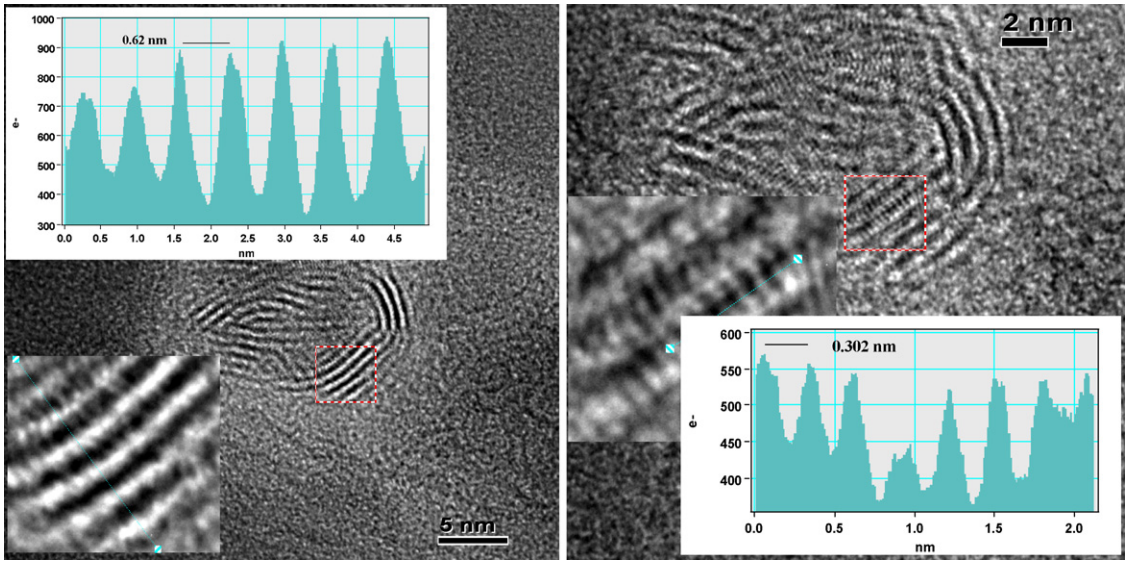

Fig. 10. High-resolution TEM (magnified) micrograph of a high silica sulfided NiMo supported catalyst (NiMoAS-5) along with well sulfided slab distances of metal crystallites.

edges sites (Ni–S, 0.221 nm) so the HDS activity. Thus, the aggregation of MoS_2 is not only the cause for the decrease in HDS activity but also decrease in the edge sites of the MoS_2 is also responsible. The crystallographic distances from Fig. 10 have been corroborated to the Ni–Ni, Mo–Mo or even Ni–Mo metal–metal interaction. Such slabs are characteristically observed for high SiO_2 supported catalysts which further specify that silica promotes weak interaction between metal-support or crystal growth of active phases.

4. Conclusion

High specific surface area, mesoporous Al_2O_3–SiO_2 mixed oxide supports were prepared by sol–gel homogeneous co-precipitation method at a nanoscale level of distribution of Al and Si elements. The mixing of SiO_2 with Al_2O_3 modifies the textural properties and interaction behavior towards MoS_2 phases and consequently affects the catalyst activity. The activity results on supported catalysts indicated that introduction of SiO_2 into Al_2O_3 modifies the metal support interaction of sulfided active metals species, which varies the catalytic activity. The characterization results showed that the effect of support is responsible to form different catalytic sites. An increase of SiO_2 content in the support promotes the crystallization of MoO_3 phases and a relatively longer crystal of MoS_2 in the sulfided catalysts. The decrease in activity is not only due to the molybdenum crystallization but also to a decrease in the edge sites (promoted sites) of the MoS_2.

Acknowledgements

One of us C. Leyva thanks to IMP for master and doctorate fellowships. We also express our gratitude to Dr. C. Angeles Chavez for HRTEM analysis.

References

[1] M.S. Thompson, European Patent 0181035, assigned to Shell Int. Res. (1986).
[2] E. Lecrenary, K. Sakanishi, I. Mochida, T. Suzuka, Appl. Catal. A: Gen. 175 (1998) 237–243.
[3] M.S. Rana, S.K. Maity, J. Ancheyta, G. Murali Dhar, T.S.R. Prasada Rao, Appl. Catal. A: Gen. 253 (2003) 165–176.
[4] N. Kunisada, K.-H. Choi, Y. Korai, I. Mochida, K. Nakano, Appl. Catal. A: Gen. 273 (2004) 287–294.
[5] N. Kunisada, K.-H. Choi, Y. Korai, I. Mochida, K. Nakano, Appl. Catal. A: Gen. 279 (2005) 235–239.
[6] J. Scherzer, A.J. Gruia, Hydrocracking Science and Technology, Marcel Dekker, New York, 1996.
[7] A. Nishijima, H. Shimada, T. Sato, Y. Yoshimura, J. Hiraishi, Polyhedron 5 (1986) 243–247.
[8] Y. Okamoto, M. Breysse, G. Murali Dhar, C. Song, Catal. Today 86 (2003) 1–3.
[9] M. Breysse, J.L. Portefaix, M. Vrinat, Catal. Today 10 (1991) 489–505.
[10] G. Muralidhar, F.F. Massoth, J. Shabtai, J. Catal. 85 (1984) 44–52.
[11] G.A. Parks, Chem. Rev. 65 (1965) 177–198.
[12] M. Kosmulski, J. Colloid Interface Sci. 298 (2006) 730–741.
[13] N. Ushifusa, M.J. Cima, J. Am. Ceram. Soc. 74 (1991) 2443–2447.
[14] V.M. Gunko, V.I. Zarko, V.V. Turov, R. Leboda, E. Chibowski, E.M. Pakhlow, E.V. Goncharuk, M. Marciniak, E.F. Voronin, A.A. Chuiko, J. Colloid Interface Sci. 220 (1999) 302–323.
[15] L. Qu, W. Zhang, P.J. Kooyman, R. Prins, J. Catal. 215 (2003) 7–13.
[16] B. Pawelec, R.M. Navarro, J.M. Campos-Martin, A. López Agudo, P.T. Vasudevan, J.L.G. Fierro, Catal. Today 86 (2003) 73–85.
[17] O. Weisser, S. Landa, Slphide Catalyst—Their Properties and Application, Programon Press, Oxford, New York, 1971.
[18] M.S. Rana, J. Ramírez, A.G. Alejandre, J. Ancheyta, L. Cedeño, S.K. Maity, J. Catal. 246 (2007) 100–108.
[19] H. Makishima, Y. Tanaka, Y. Kato, S. Kure, H. Shimada, N. Matsubayashi, A. Nishijima, M. Nombra, Catal. Today 29 (1996) 267–271.
[20] M.A. Ali, T. Tatsumi, T. Musada, Appl. Catal. A: Gen. 233 (2002) 77–90.
[21] V. La Parola, G. Deganello, A.M. Venezia, Appl. Catal. A: Gen. 260 (2004) 237–247.
[22] V. La Parola, G. Deganello, C.R. Tewell, A.M. Venezia, Appl. Catal. A: Gen. 235 (2002) 171–180.
[23] S.J. Gregg, K.S.W. Sing, Adsorption, Surface Area and Porosity, Academic Press, London, 1991.
[24] H. Jeziorowski, H. Knozinger, P. Grange, P. Gajardo, J. Phys. Chem. 84 (1980) 1825–1829.
[25] P. Dufresne, E. Payen, J. Grimbolt, J.P. Bonnelle, J. Phys. Chem. 85 (1992) 2344–2351.
[26] H. Hu, I.E. Wachs, J. Phys. Chem. 99 (1995) 10897–10910.
[27] S. Rajagopal, H.J. Marini, J.A. Marzari, R. Miranda, J. Catal. 147 (1994) 417–428.
[28] M.S. Rana, M.L. Huidobro, J. Ancheyta, M.T. Gómez, Catal. Today 107/108 (2005) 346–354.
[29] R. Prins, in: I.E. Wachs, L.E. Fitzpatrick (Eds.), Characterization of Catalytic materials, Butterworth-Heinemann, USA, 1992, , Chapt. 6.
[30] C. Leyva, M.S. Rana, F. Trejo, J. Ancheyta, Catal. Today, communicated.
[31] K. Bourikas, C. Kordulis, A. Lycourghiotis, Catal. Rev. Sci. & Eng. 48 (2006) 363–444.
[32] S. Eijsbouts, Appl. Catal. A 158 (1997) 53–92.
[33] Y. Sakashita, Y. Araki, K. Honna, H. Shimada, Appl. Catal. A: Gen. 197 (2000) 247–253.
[34] S. Srinivasan, A.K. Datye, C.H.F. Peden, J. Catal. 137 (1992) 513–522.
[35] S. Eijsbouts, L.C.A. van den Oetelaar, R.R. van Puijenbroek, J. Catal. 229 (2005) 352–346¤.
[36] H. Topsøe, B.S. Clausen, F.E. Massoth, Hydrotreating Catalysis Science and Technology, Springer-Verlag, New York, 1996.
[37] P.L. Hansen, H. Topsøe, J.-D. Malm, Proc. ICEM 13, Paris, (1994), p. 1077.
[38] S.P.A. Louwers, R. Prins, J. Catal. 133 (1992) 94–111.